# Chapter 2

# Literature Review

## 2.1. Introduction to one-dimensional ZnO nanostructures

Research concerning 1D nanomaterials started when carbon nanotubes were discovered by Iijima (1991), silicon NWs were grown by Lieber's group (1998), and ZnO NWs and NBs were found by Wang's group from Georgia Tech (Pan *et al.*, 2001).

### 2.1.1. Discovery of ZnO nanobelts (2001)

Figure 2.1 shows ZnO nanobelts that were grown by Wang's group. After discovering a few key ZnO nanostructures, the Wang group turned toward understanding their formation process and growth.

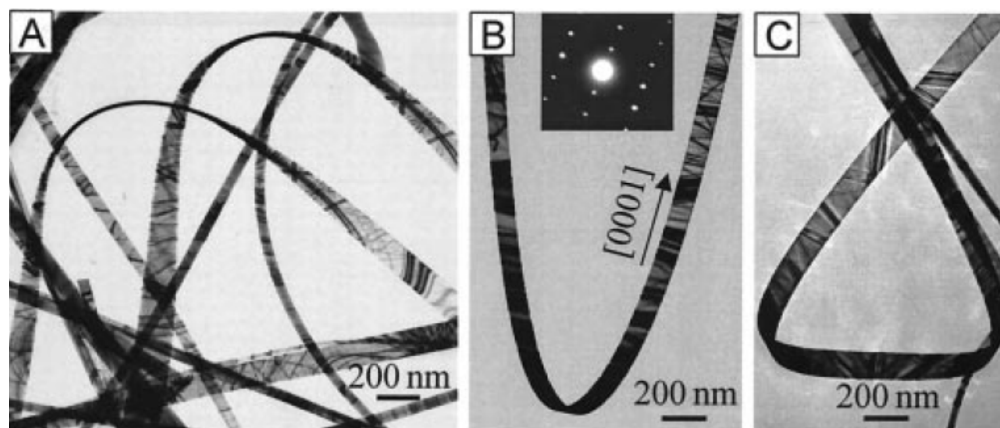


**Figure 2.1.** TEM images of the as-synthesized ZnO nanobelts (Pan *et al.*, 2001).

In fact, ZnO nanobelts with a rectangular cross section in a ribbon-like morphology are very promising for sensors, field emission, piezoelectric, and *p-n* junction due to the fact that the surface-to-volume ratio is very high (Yang, Y. *et al.*, 2009; Lao *et al.*, 2007; Wan *et al.*, 2008; Yang, Y. *et al.*, 2008; Cheng *et al.*, 2006; Chen, C.H., *et al.*, 2009; Arnold *et al.*, 2003; Kong & Wang, 2003). Therefore, investigation about properties of the ZnO nanobelts could lead to different application.

Spring morphology of the ZnO nanostructure was also fabricated by the Wang group. This was made a single NB that was dominated by (0001) polar surfaces (Fig. 2.2(a)) (Kong & Wang, 2003; Ding *et al.* 2004). This group gained an understanding of the formation of these nanostructures using a crystalline NB after careful microscopy. They demonstrated that, the polar charges on NB surfaces induced their shape and proposed a model to explain the formation of the nanospring.

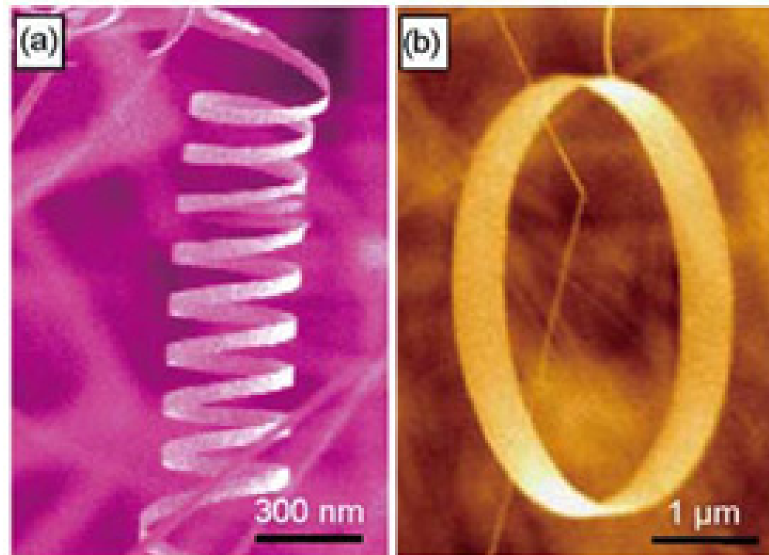


**Figure 2.2.** SEM images of (a) single-crystal nanospring (Kong & Wang, 2003), (b) nanoring (Ding *et al.* 2004).

These researchers also obtained another nanostructure of ZnO; freestanding, single-crystal, completely closed nanorings (Fig. 2.2(b)). After an in-depth study of the nanoring structure by high-resolution transmission electron microscopy (HRTEM), they discovered the structure and formation process of the nanoring (Kong *et al.*, 2004). Nanoring formation appears to be initiated by circularly folding a NB, which is caused by long-range electrostatic interaction. Co-axial and uni-radius loop-by-loop winding of the NB forms a complete ring. Short-range chemical bonding among the loops results in a single crystal structure. This self-coiling is likely to be driven by a minimization of the

energy contributed by polar charges, surface area, and elastic deformation. This is a second example of the polar surface-dominated growth phenomenon.

### 2.1.2. Growth of aligned ZnO nanowires (2004—2005)

NBs are typically randomly grown on a substrate. For practical applications, the growth of aligned nanowires arrays is more attractive. The Wang group also carried out the growth of NWs arrays on sapphire via the vapor phase (Fig. 2.4) (Wang, Z.L. *et al.,* 2004).

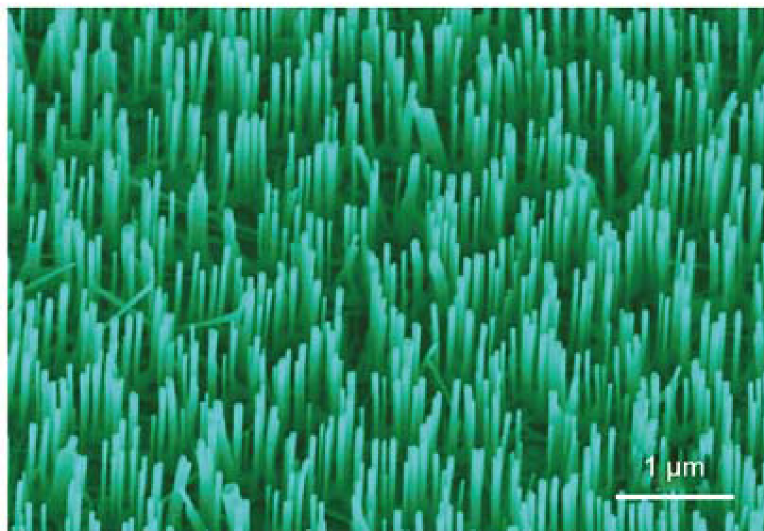


**Figure 2.3.** Aligned ZnO nanowire arrays that were grown on a sapphire surface (Wang, Z.L. *et al.,* 2004).

This group used a sapphire crystal as the substrate and gold dots that were deposited on the surface using a soft lithography patterning technique. In this manner, aligned nanowires were achieved at a growth temperature of ~900 °C.

### 2.1.3. Doping of ZnO nanostructures

It is well known that the doping of impurities, using selected elements into semiconductors greatly affects their basic physical properties, (e.g., electrical, optical,

and magnetic properties), which are crucial for their practical application. The impurities that are doped into ZnO can be defined by four types:

i) Doping with donor impurities to obtain high *n*-type conductivity;

ii) Doping with acceptor impurities to obtain *p*-type conductivity;

iii) Doping with rare-earth elements to obtain better optical properties; and

iv)Doping with transition metals to obtain desired magnetic properties (Djurisˇic´ & Leung, 2006).

ZnO with a wurtzite structure is known to be an *n*-type semiconductor. This is because of its deviation from stoichiometry, owing to the presence of intrinsic defects, including Zn interstitials ($Zn_i$), Zn vacancies ($V_{Zn}$), O interstitials ($O_i$) and O vacancies ($V_O$). Based on these reasons, undoped ZnO shows intrinsic *n*-type conductivity with very high electron densities of about $10^{21}$ $cm^{-3}$ ( zgur *et al.*, 2005). Therefore, *n*-type doping of ZnO is relatively easier than *p*-type doping.

Groups III (Yun *et al.*, 2010; Lin, S *et al.*, 2008; Chen, J.T., *et al.*, 2009; Lo *et al.*, 2009; Lee *et al.*, 2009; Gupta *et al.*, 2009; Ahn *et al.*, 2009a; Li *et al.* 2007) and IV (Deng, *et al.*, 2007; Deng & Zhang, 2008; Su *et al.*, 2009; Das *et al.*, 2009; Su *et al.*, 2008; Zhou *et al.*, 2005a; Li *et al.* 2004) of the periodic table are typically used as donor impurities to dope ZnO; they can substitute for Zn. Many studies have already been performed regarding the synthesis and characterization of ZnO nanostructures doped with group three elements (Bae, *et al.*, 2005a,b). Because indium doping is important for the conductor industry, many research groups focus on the development of ZnInO nanostructures with excellent properties (Jung, M.N *et al.*, 2009; Pál *et al.*, 2009). ZnInO films show similar electrical conductivity and better transparency in both the visible and the infrared (IR) regions compared with ITO. Thus, they can be widely used as transparent conductors in many applications (Peng *et al.*, 2009). Furthermore, indium is one of the best elements for the band-gap engineering of ZnO, provided that the

content is carefully controlled (Huang, Y. *et al.*, 2007; Xu *et al.*, 2006; Lee *et al.*, 2009; Gupta *et al.*, 2009; Jie *et al.*, 2004a; Jie *et al.*, 2004b). Al-doped ZnO nanostructures can raise electrical conductivity of ZnO and shift its luminescence peaks to higher or lower energies (Lin, Y.H *et al.*, 2008; Lo *et al.*, 2009; Ortega *et al.*, 2009).

Halogen elements are used as substitution elements for O and can also serve as donors in the ZnO structure. Furthermore, these elements reduce oxygen adsorption on surfaces (Cui *et al.*, 2008). In addition to halogen elements, chalcogens elements (e.g., O, S, Se, and Te) can be substituted for O. Sulfur (S) has many physical and chemical properties that are similar to those of oxygen, due to a the similar structures of their electronic shells. Therefore, as an anion dopant, S can easily substitute for O. S is one of the best dopant elements for affecting visible emission of ZnO. In fact, S-doped ZnO is expected to modify the electrical and optical properties of ZnO because of the large electronegativity and size differences between S ($r_S^{2-}$ =0.18nm) and O ($r_O^{2-}$=0.14nm) (Zhang, X. *et al.*, 2009; Kar *et al.*, 2009; Hussain *et al.*, 2007a). In fact, not only can S-doped ZnO nanostructures be used as a single source in the visible region, but band-gap engineering may allow the content of S to be controlled in ZnO (Bae *et al.*, 2004)

There are several factors that contribute to the difficulties associated with *p*-type doping of ZnO. First of all, dopants might be compensated by low-energy native defects (Walukiewicz, 1994). Second, the low solubility of the dopant in wide-band-gap materials, such as ZnO, is another possibility. Finally, deep impurity levels can be another source of doping problems, as they cause significant resistance to the formation of a shallow acceptor level (Özgür *et al.*, 2005). Elements from groups I (Jayanthi *et al.*, 2009; Nayak *et al.*, 2009; Huang, G-Y *et al.*, 2009) and V (Li *et al.*, 2008; Yao *et al.*, 2009; Yu *et al.*, 2009; Sui *et al.*, 2009; Wang, Q. *et al.*, 2009; Yu *et al.*, 2008; Yu *et al.* ,2009) typically serve as acceptor impurities in ZnO. Due to electronic structure and atomic size considerations, nitrogen has been applied as the most suitable impurity for

*p*-type doping in ZnO. However, several experimental efforts by many different groups have not been able to demonstrate a stable and reproducible *p*-type material. Recently, based on advanced first-principles calculations, Lyons *et al.* (2009) found that nitrogen is actually a *deep* acceptor and hence cannot lead to hole conductivity in ZnO. In fact, group-I elements (Li, Na, and K) can substitute at Zn sites and group-V elements (N, P, and As) can substitute at O sites. Silver (Ag) can also be applied as an acceptor impurity in ZnO (Song *et al.*, 2009).

In addition to donors and acceptors impurities in ZnO, ZnO nanostructures have also been doped with some rare-earth elements, including Ce (Cheng *et al.*, 2008; Yang, J. *et al.*, 2008), Pr (Jayanthi *et al.*, 2009), Nd (Subramanian *et al.*, 2009), Eu (Zhang, Y. *et al.*, 2009; Pan *et al.*, 2009), Tb (Jia *et al.*, 2009), and Dy (Wu *et al.*, 2006). An important factor in the optical analysis of rare-earth-doped ZnO nanostructures is the characterization of excitation wavelength, which is performed using a photoluminescence (PL) spectrometer. When doping is achieved using rare-earth elements, it is possible that their emission will be masked by ZnO defect emission. Therefore, the excitation wavelength must be carefully chosen to establish the effects of doping on the optical properties of the material (Djurisˇic´ & Leung, 2006).

By alloying ZnO with another material that has a different band-gap, the band-gap of ZnO can be fine tuned, thus affecting the exciton emission wavelength. MgO and CdO are two suitable materials for band-gap tuning of ZnO over a wide range. This is due to the large difference between their band-gaps and the ZnO band-gap. In addition, the alloying of ZnO with MgO or Mg with CdO or Cd creates $Zn_{1-x}Mg_xO$, and $Zn_{1-y}Cd_yO$, respectively, which are potential candidates for future optoelectronic devices. The addition of MgO, which has a larger band-gap (7.7 eV) than ZnO, results in a widened band-gap (Zhu, *et al.* 2006; Wang. F *et al.,* 2009; Heo, *et al.,* 2003; Kling *et al.*, 2004; Park *et al.*, 2004; Yang, A.L, *et al.*, 2009; Zeng *et al.*, 2008; Ahn *et al.*,

2009c; Qiu *et al.*, 2008; Hsu, *et al.* 2006; Pan *et al.* 2007, Tang *et al.* 2006, Wei *et al.* 2008; Zhang *et al.* 2007). On the other hand, CdO decreases the band-gap of ZnO due to its smaller band-gap (2.3 eV) compared with ZnO (Vijayalakshmi *et al.*, 2008; Zhou *et al.*, 2006).

Magnetic properties of ZnO nanostructures are also changed by doping with transition materials, including Sc (Zhou *et al.*, 2005b), V (Chen *et al.*, 2010; Luo *et al.,* 2009), Cr (Schneider *et al.*, 2009), Mn (Huang, X *et al.*, 2009; Straumal *et al.*, 2009), Fe (Gautam *et al.*, 2009; Liu *et al.*, 2009), Co ( Patra *et al.*, 2009; Loan *et al.*, 2009), Ni (Iqbal *et al.*, 2009), Cu (Xu *et al.*, 2010), and Nb (Feng *et al.*, 2009). In addition, some comparative studies concerning the effects of these elements on ZnO nanostructures properties have been reported (Phan *et al.*, 2008; Müller *et al.*, 2009; Tamura & Ozaki, 2009).

## 2.2. Fundamental properties and theoretical models

In this section, the fundamental properties of the ZnO are presented. Special attention is paid to the characteristic of the band gap energy and optical property. Table 2.1 shows some imprtant parameters of ZnO.

**Table. 2.1.** Selective material parameters of ZnO.
(http://www.semiconductors.co.uk/propiivi5410.htm#ZnO,ZnS,ZnSe,ZnTe)

| Crystal structure | Wurtzite (stable phase at 300 K), Zinc blend, Rocksalt |
|---|---|
| Lattice parameters | $a_0$=0.32495 nm, $c_0$=0.52069 nm, $c_0/a_0$=1.602 |
| Wurtzite nearest neighbor Dist. at 300K calculated as $0.375c_0$ which would be correct in ideal hexagonal structure of $c_0/a_0$=1.633 | 0.195 nm |
| Wurtzite density at 300K | 5.606 $g/cm^3$ |
| Melting point | 1975 C |
| Thermal conductivity $W.cm^{-1}.^{o}C^{-1}$ | 0.6 |
| Specific heat in cal/gm | 0.125 |
| Linear expansion coefficient in $^{o}C^{-1}$ for wurtzite structure | $a_0$: $6.5x10^{-6}$ $c_0$: $3.0x10^{-6}$ |
| Exciton Bohr radius | $a_B$ = 2.34 nm |
| Zinc-blende structure refractive index:<br>Wurtzite structure refractive index: | 2.008<br>2.029 |
| Energy gap $E_g$ at 300 K;<br>Zinc blende structure:<br>Wurtzite structure: | <br>3.37 eV (at 300 K), Direct,<br>3.4376 eV (at 4.2 K) |
| Exciton binding energy | 60 meV |
| Electron effective mass | $0.24m_0$ |
| Electron Hall mobility at 300 K for low n-type conductivity | 200 $cm^2/Vs$ |
| Point group | $C^4_{6v}$ (6mm) (Wurtzite) |

### 2.2.1. Crystal structure of ZnO

Most of the group II-VI binary compound semiconductors crystallize in either cubic, zinc-blende, or hexagonal wurtzite structure where each anion (O elements in ZnO structure) is surrounded by four cations (Zn elements in ZnO structure) at the corners of a tetrahedron, and vice versa. This tetrahedral coordination is typical of $sp^3$ covalent bonding, but these materials also have a substantial ionic character. Therefore, ZnO as one of the II-VI compound semiconductors has these crystal structures that is shown in Fig. 2.5, schematically. At ambient conditions, the thermodynamically stable phase is hexagonal. The zinc-blende ZnO structure can be formed only by growth on cubic substrates, and the rocksalt (NaCl) structure may be obtained at relatively high pressures (Özgür *et al.*, 2005).

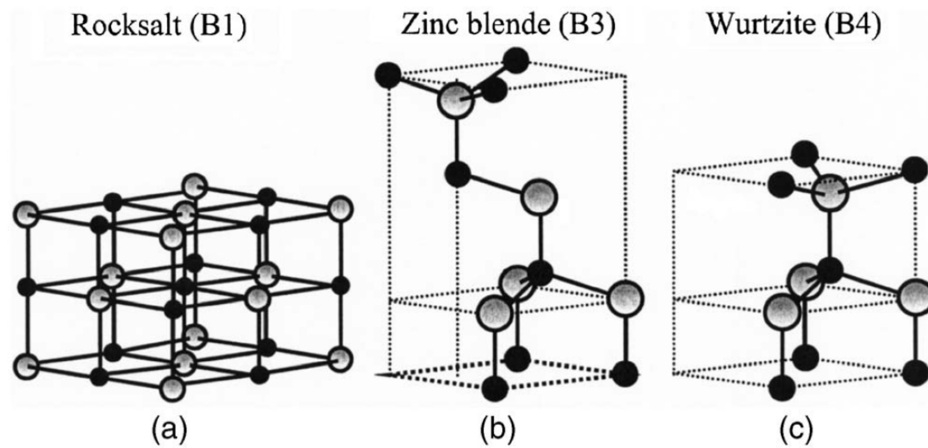


**Figure. 2.4.** Stick and ball representation of ZnO crystal structures: (a) cubic rocksalt ($B_1$) , (b) cubic zinc blende ($B_3$), and (c) hexagonal wurtzite ($B_4$). The shaded gray and black spheres denote Zn and O atoms, respectively (Özgür *et al.*, 2005).

The hexagonal structure of ZnO has two important characteristics: non-central symmetry and the polar surfaces. The hexagonal structure of ZnO can be described as a number of alternating planes composed of tetrahedrally coordinated $O^{2-}$ and $Zn^{2+}$ ions, stacked alternatively along the *c*-axis (Fig. 2.6).

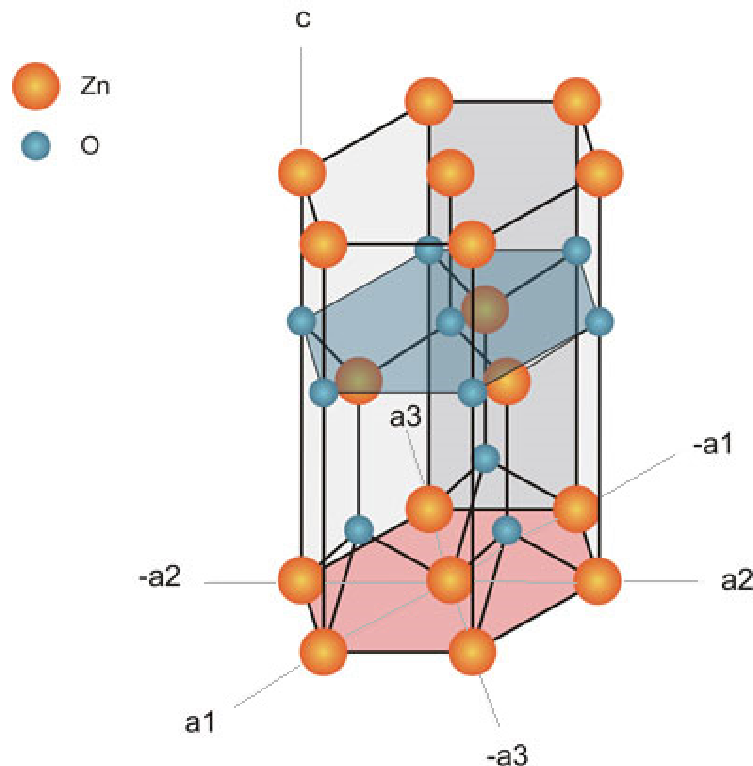


**Figure 2.5.** The hexagonal wurtzite structure of ZnO. (http://www.emg.tu-bs.de/bilder/forschung/material/zno.jpg)

The oppositely charged ions produce positively charged (0001)-Zn and negatively charged (000-1)-O polar surfaces.

### 2.2.2. Optical properties

The optical properties of a semiconductor are affected by both intrinsic and extrinsic effects. Intrinsic optical transitions happen between electrons in the conduction band and holes in the valance band, including excitonic effects due to Coulomb interactions. Excitons are classified into two types, including free and bound excitons (Özgür *et al.*, 2005). In high-quality samples with low impurity concentrations, the free exciton can also exhibit excited states, in addition to their ground-state transitions. Extrinsic properties are connected to dopants or defects, which usually generate discrete electronic states in the band gap and, therefore affect both optical-absorption and emission processes (Özgür *et al.*, 2005). The semiconductor material plays a significant role in the electronic states of the bound excitons (BEs) and, in particular, in the band structure. Theoretically, excitons could be bound to neutral or charged donors and acceptors (Özgür *et al.*, 2005).

#### 2.2.2.1. Band-gap engineering of ZnO

For the ternary semiconductor $A_xZn_{1-x}O$ (where A = Mg or Cd) as a function of the composition of A, x, can be expressed by the following formula (Jagadish & Pearton, 2006):

$$E_g(x) = (1-x)E_{ZnO} + xE_{AO} - bx(1-x) \quad (2\text{-}1)$$

where

$E_{ZnO}$ is the band-gap energy (eV) of ZnO

$E_{AO}$ is the band-gap energy (eV) of AO, and

b is the band-gap bowing parameter (eV).

The physical origin of the bowing parameter can be caused by disorder effects that are created by the presence of different cations or anions (Van Vechten & Bergstresser, 1970). The physical origin of bowing has been investigated using first principle calculation ( Bernard & Zunger, 1987). This calculation is able to identify three major contributions toward this parameter (Wenckstern *et al.*, 2009):

i) Replacement of the lattice constants of the binary constituents, because, the alloy causes a volume deformation of the band structure;

ii) Charge exchange in the alloy relative to its constituent binary subsystem a chemical-electronegativity contribution change, and

iii) A structural contribution due to the relaxation of the anion-cation bond lengths in the alloy.

#### 2.2.2.2. Burstein-Moss effect

The minimum energy needed to excite an electron from the valance band to the conduction band is defined as the optical gap in semiconductors. In undoped semiconductors the optical gap equals the energy separation $E_{g0}$ between the band edges, as shown for the case of isotopic and parabolic bands in Fig. 2.7 (a). In a doped semiconductor, the bottom states of the conduction band are occupied by the donor electrons. Optical transitions are vertical because the Pauli Exclusion Principle prevents states from being doubly occupied. In fact, the optical gap is given by the energy difference between states with Fermi momentum in the conduction and valance bands. This configuration is shown in Fig. 2.7 (b) (Sernelius *et al.*, 1988). The blocking of the low-energy transitions is known as the Burstein-Moss (BM) effect; this effect increases the energy of the optical gap (Burstein, 1954; Moss, 1954):

$$\Delta E_g^{BM} = \frac{h^2}{8\pi^2}(3\pi^2 n)^{2/3}\left[\frac{1}{m_e^*}+\frac{1}{m_h^*}\right] \qquad (2\text{-}2)$$

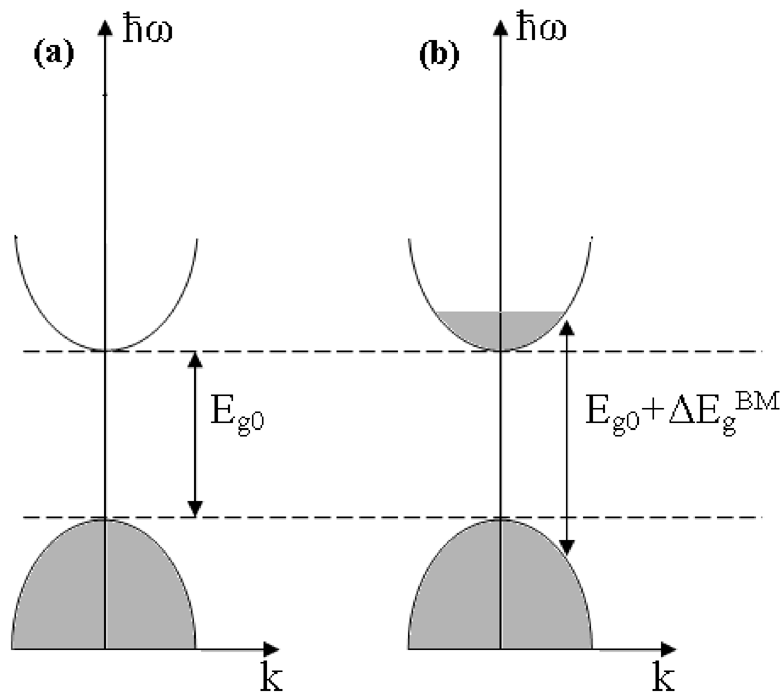


**Figure. 2.6.** Schematic of the band-gap in (a) a pure state and (b) a doped state.

where *h* is the Planck constant, *n* is the electron density measured at different doping concentrations. $m_h^*$ and $m_e^*$ are the effective masses for holes in the valance band and electrons in the conduction band, respectively. Consequently, the measured band gap determined from the onset of inter-band absorption moves to a higher energy (i.e., undergoes "a blue shift"). According to Equation (2-2), the band gap increases as the carrier concentration increases.

### 2.2.3. Photoluminescence

Photoluminescence (PL) study is a very helpful method for studying the band gap of semiconductors and band-gap engineering. The band gap of semiconductors, as well as the effects of doping materials on the band gap, can be measured by PL spectroscopy. A fundamental physical characteristic of PL is the spontaneous emission of a photon from a material under optical excitation. Therefore, PL spectroscopy is a non-destructive, contactless method and a very sensitive tool for the study of electronic

transitions in semiconductors. A large amount of information can be obtained about a semiconductor material via PL measurements including: the band-gap energy, defects, presence of impurities, and optical quality.

In PL, when a semiconductor material is excited by an excitation source (usually a laser) having an energy above the band gap of the material, photons from the source are absorbed and caused electrons within the material to move into allowable excited states (in the conduction band). Then, these electrons return to their equilibrium states (ground states). This process is shown schematically in Fig. 2.7. These transitions occur via two processes: radiative transition (luminescence) and non-radiative transition (phonon emission) (Smith, 1981). Figures 2.8 (a)-(d) show all of the radiative electronics transitions and Fig 2.8 (e) shows the non-radiative electron transition after excitation of the semiconductor material. The PL power, excitation level, and temperature are directly related to the dominant recombination process. In general, a non-radiative recombination is associated with localized defect levels, which can determine the material quality.

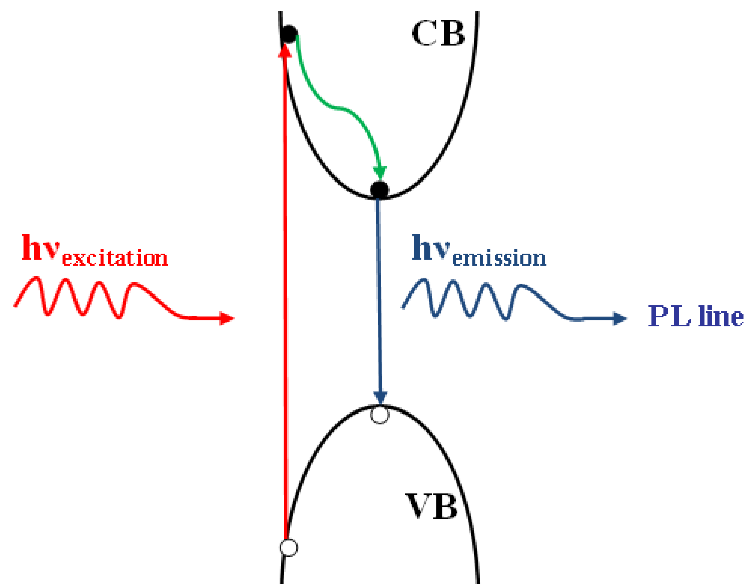


**Figure 2.7.** Schematic of the typical PL process.

Therefore, quantifying the amount of radiative recombination can indicate the quality of a material. In general, all characterized ZnO materials show two bands by room temperature PL spectroscopy: one centered around 380 nm (3.26 eV) in the ultraviolet (UV) region and the other between 450 nm (2.75 eV) and 600 nm (2.06 eV) in the visible region of electromagnetic spectrum. The UV emission is also called the near band edge (NBE) emission due to the recombination of free excitons through an exciton–exciton collision process (Fig 2.8 (a)). The visible emissions of ZnO materials are also called deep level emissions (DLEs), which have different origins.

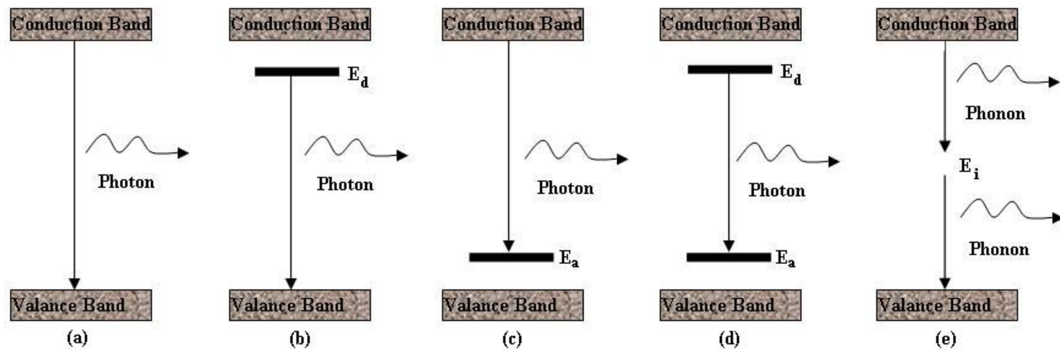


**Figure 2.8.** Radiative recombination process: (a) band to band, (b) donor to valance band, (c) conduction band to acceptor, (d) donor to acceptor, and (e) non-radiative process via an intermediate state.

Figure 2.9 shows a schematic band diagram of DLEs in ZnO based on the full potential linear muffin-tin orbital method and reported data (Ahn *et al.*, 2009b).

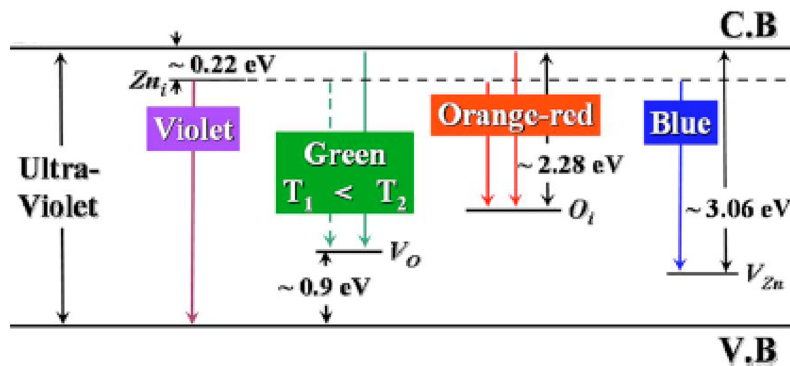


**Figure 2.9.** Schematic band diagram of DLEs in ZnO nanostructures based on the full potential linear muffin-tin orbital method and reported data (Ahn *et al.*, 2009b).

The DLEs of ZnO nanostructures were found to be strongly dependent on the growth conditions and growth methods used (Ahn *et al.*, 2009b). The blue emission is linked to radiative defects at the interface of the components of ZnO urchins (Lin *et al.*, 2001; Jin *et al.*, 2000) or to the existence of interstitial zinc ($Zn_i$) in the ZnO lattices (Zeng *et al.*, 2005). The green band emission has been suggested to corresponds with the singly ionized oxygen vacancy ($V_O$) in ZnO and results from the recombination of a photo-generated hole with the singly ionized charge state of this defect (Vanheusden *et al.*, 1996). In addition, Liao *et al.*, (2008) suggested that oxygen vacancies are strongly responsible for the visible emission of ZnO. In fact, oxygen vacancies occur in three charge states (Liao *et al.*, 2008):

i) The doubly ionized oxygen vacancy $V_O^{++}$ , which does not capture any electrons and is doubly positively charged relative to the lattice of ZnO**;**

ii) The singly ionized oxygen vacancy $V_O^{+}$, which has captured one electron and is singly positive charged relative to the lattice of ZnO; and

iii) The neutral oxygen vacancy $V_O^{\chi}$, which has captured two electrons and is neutral relative to the lattice of ZnO.

According to these levels:

i) Recombination of the $V_O^{++}$ trapped center with delocalized electrons close to the conduction band is responsible for the yellow emission;

ii) The electron transition from $V_O^{+}$ centers on the valance band edge; and

iii) The electron transition from $V_O^{\chi}$ centers on the valance band edge.

These emissions are shown in Fig. 2.10.

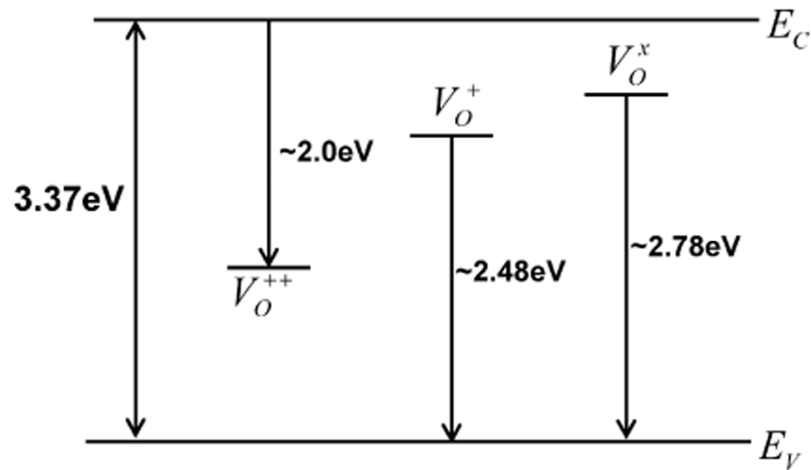


**Figure 2.10.** Schematic of the three visible emission processes, which show energy levels of O vacancies in ZnO structure (Liao *et al.*, 2008).

**2.2.3.1. Surface effects on photoluminescence properties**

The study of the size effect on the properties of nanostructures is of great importance. Nanostructure materials show a high surface-to-volume ratio, which critically affects their electronic and optical properties, especially near their band gaps (Barnard *et al.*, 2003). The effect of size on the optical properties of ZnO nanorods (Chen *et al.*, 2006), nanobelts (Wang, Z.L 2004), and nanoclusters (Antony *et al.*, 2005) has been reported in the literature. In fact, in nanostructures, the surface-to-volume ratio is bigger than for bulk materials; therefore, surface atoms play a significant role in the properties of nanostructures. Based on this, Shalish *et al.* (2004) have investigated the effects of this ratio on the optical properties of ZnO nanowires. They reported size-dependent surface luminescence in ZnO nanowires using a simple mathematical model and obtained a relationship between nanowire radius and luminescence peak intensity ratio. These researchers observed significantly different results for the optical properties of a bulk ZnO wafer and ZnO nanowires. This model was based on a surface-recombination-layer approximation, which assumes a layer around a wire (diameter *r*,

length $l$, and $l \gg r$) with thickness $t$. In this configuration, the volume associated with the wire surface, $V_S$, is:

$$V_S = l\pi[r^2 - (r - t)^2] \quad (2\text{-}3)$$

The remaining volume of the wire, $V_B$, associated with the bulk, is then:

$$V_B = l\pi (r - t)^2 \quad (2\text{-}4)$$

The ratio between these volumes is:

$$\frac{V_B}{V_S} = \frac{r^2}{2rt - t^2} - 1 \quad (2\text{-}5)$$

This equation shows a nearly linear relationship between the wire radius and the volume ratio of wire materials. In the work of these authors, a relationship was obtained between the above ratio and the ratio between the band-edge (BE) and below-band-edge (BG) luminescence peak intensities ($I_{BE}/I_{BG}$):

$$\frac{I_{BE}}{I_{BG}} = C(\frac{r^2}{2rt - t^2} - 1) \quad (2\text{-}6)$$

where C is a constant. Therefore, according to this equation, visible emissions dominate emissions in PL results for nanowires with smaller diameters.

In addition, Chen *et al.* (2006) obtained a relationship between the volume ratio of the wire material and the energy shift for the band-gap of ZnO nanorods using cathodeluminescence (CL) spectroscopy. They have also suggested that the surface-to-volume ratio plays a significant role in this shift. These researchers found that:

$$\Delta E_g(shift) = E_g^{CL} - E_g^{bulk} \propto R = 4t / r \quad (2\text{-}7)$$

Based on this equation, wires with smaller diameters show bigger band-gap than those having bigger diameters. Chen *et al.* (2006) showed that this equation is correct for wires having diameters $r < 620$ nm, and wires with diameters bigger than 620 nm will exhibit bulk-like properties, with no observed shift in energy.

In addition to the above phenomena, the quantum confinement effect is another effect that size has on the optical properties of ZnO nanostructures. The quantum

confinement effect occurs when one or more of the nanostructure dimensions are smaller than the Fermi wavelength. In this time, the boundary conditions of holes and electrons are restricted to one or more dimensions (Ren, 2006). In the current application, nanostructures having different shapes have restrictions in different dimensions: a quantum dot (QD) such as a small sphere, has confines in all three dimensions (3D); a quantum wire has confines in two dimensions (2D); and a quantum well has confines in one dimension (1D). Quantum confinement is responsible for the increase in energy difference between energy states and the band gap in semiconductors having ultra-small sizes (Stichtenoth *et al*., 2007). A particle behaves as if it were free when the confining dimension is large compared to the wavelength of the particle. During this state, the band-gap remains at its original energy, owing to the presence of a continuous energy state. However, as the confining dimension decreases and reaches a certain limit, typically at the nanoscale, the energy spectrum becomes discrete. As a result, the band-gap becomes size dependent. This ultimately results in a blue shift in optical illumination as the size of the particles decreases. Specifically, the effect describes the phenomenon that results from electrons and electron holes being squeezed into a dimension that approaches a critical quantum measurement, called the exciton Bohr radius. Therefore, this effect will be dominant in the ZnO nanostructure when their size is comparable with the ZnO exciton Bohr radius ($a_B \approx 2.34$ nm; Senger & Bajaj, 2003). In fact, this phenomenon has not been observed for nanowires with diameters bigger than 10 nm (Gu *et al.*, 2004).

### 2.2.4. Vibrational properties and Raman spectroscopy

According to group theory, single crystalline ZnO belongs to the $C^4_{6V}$ ($P6_3mc$) space group, having two formula units per primitive cell and eight sets of optical phonon modes at the Γ point of the Brillouin zone (BZ). Figure 2.11 shows the BZ of

the hexagonal wurtzite structure. The phonon modes according to group theory, at the BZ center for hexagonal structure are given by (Ferraro *et al.,* 2003):

$$\Gamma = 2A_1 + 2E_1 + 2E_2 + 2B_1 \quad (2\text{-}8)$$

They are classified as $A_1$+$E_1$+$2E_2$ modes, which are Raman active; $A_1$+$E_1$ modes, which are infrared (IR) active; and $B_1$ modes, which are silent (neither Raman nor IR active). The $A_1$ and $E_1$ modes are polar, and split into transverse optical (TO) and longitudinal optical (LO) branches; the $E_{2H} – E_{2L}$ mode indicates the presence of pure ZnO that can only be found when the ZnO is a single crystal (Umar, & Hahn, 2006). The $E_2$(high) mode of the Raman active mode is a characteristic peak for the wurtzite hexagonal phase of ZnO. The $E_1$(LO) mode is associated with impurities and formation defects such as oxygen vacancies (Umar *et al.*, 2005).

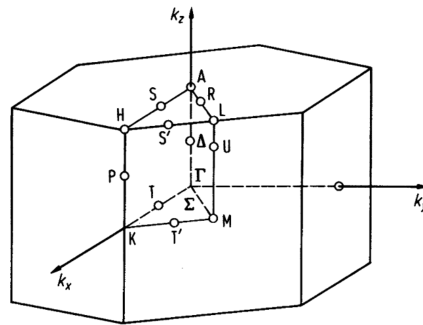


**Figure 2.11.** First Brillouin zone (BZ) of the wurtzite structure (http://www.ioffe.ru/SVA/NSM/Semicond/Append/figs/fmd21_5.gif).

Figure 2.12 shows the atomic displacement scheme of these optical modes (Harima, 2002).

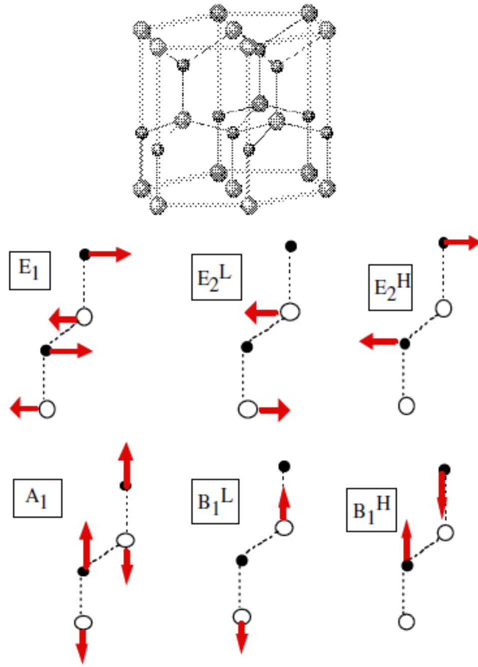


**Figure 2.12** Schematic representation of the atomic displacement of the BZ optical modes in a hexagonal lattice.

Raman spectroscopy is the best way to study of these properties. When a beam of light source (laser) is impinged upon a sample, two basic phenomena occurred. The first phenomenon is called Rayleigh scattering, where most of the photons are scattered elastically; therefore, they have the same wavelength as the incident photons (Fig. 2.13 (a)).

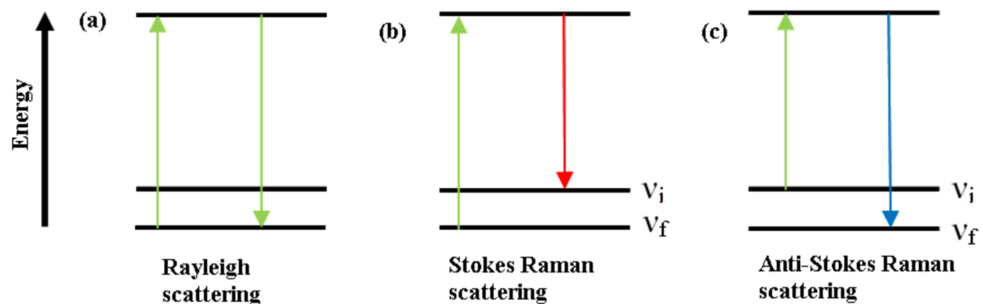


**Figure. 2.13.** Schematic diagram of different scatterings: (a) Rayleigh scattering, (b) Stokes Raman scattering, and (c) Anti-Stokes Raman scattering. The $\nu_i$ and $\nu_f$ indicate the initial and final states, respectively.

The second phenomenon is called the Raman effects, a case that a tiny portion of the photons are scattered inelastically, therefore, they have a different wavelength that is shifted from that of the original wavelength. Among these Raman scattered photons, most of them are shifted to longer wavelengths (Stokes shift) (Fig. 2.13 (b)), but a small portion are shifted to shorter wavelengths (anti-Stokes shift) (Fig. 2.13 (c)).

### 2.2.5. Field Electron Emission

The emission of electrons from the surface of a condensed phase into another phase (usually a vacuum), owing to the presence of a high electric field at the surface, is called field emission (Good & Muller, 1956). The phenomenon of field emission is associated with a quantum mechanical tunneling process whereby electrons tunnel through a potential barrier from a metal or a semiconductor under the influence of a very high applied electrostatic field, on the order of $10^7$ V/cm (0.3-0.6 V/Å) at the surface (Oostrom, 1966). As this phenomenon involves tunneling of electrons through the deformed potential barrier at the surface (ideally the tunneling can occur at 0 K), the electron emission is also termed "cold emission". The applied electric field helps to narrow the potential barrier for electrons in the emitter, allowing electrons to penetrate through it.

A high electric field near the emitter can be sufficient enough to lower the barrier, sufficiently reducing the barrier height to enable a substantial increase in emission. When the field is on the order of 0.3 V/Å, the width of the barrier is on the order of 1 nm, and electrons can be escape by tunneling, even at room temperature.

### 2.2.5.1. Fowler-Nordheim Plot (F-N Plot)

In a field electron emission experiment the measurable quantities are the field emission current ($I$) and the electric potential ($V$) applied between the cathode and the anode. The current density $J$ and electric field $E$ are related to these quantities as

$$I = J\,A \tag{2-9}$$

$$E = \beta\,V \tag{2-10}$$

where $A$ is the emitter area and $\beta$ is the field enhancement factor, which is determined by the geometry of the emitter. The Fowler-Nordheim (F-N) equation takes the following form when the above substitutions are made (Fowler & Nordheim, 1928).

$$\ln(\frac{J}{E^2}) = \ln(\frac{A\beta^2}{\varphi}) - (\frac{B\varphi^{3/2}}{\beta E}) \tag{2-11}$$

The Fowler-Nordheim equation gives the relationship between the current density $J$, the field strength $E$ and the work function $\varphi$. In this relation, $J$ is the emission current density (μA $cm^{-2}$); $E$ is the applied field (V $\mu m^{-1}$); $A = 1.56\times10^{-6}$ A eV $V^{-2}$, $B = 6.83\times10^{3}$ $eV^{-3/2}$ V $\mu m^{-1}$; $\beta$ is the field enhancement factor. The work function of emitter material was taken from the literature as 5.3 eV for ZnO (Yang, X.X. *et al.*, 2009). A plot of $\ln(I/V^2)$ versus ($10^4$/V) from this equation results in a straight line for metals and is called a Fowler Nordheim plot. The slope of this straight line is given by:

$$m = \frac{-6.8\times10^3\varphi^{3/2}s(y)}{\beta} \tag{2-12}$$

where

$$s(y) = f(y) - \frac{y}{2}\left(\frac{df(y)}{dy}\right) = 1(unity) \tag{2-13}$$

As φ, $\beta$, and $A$ are independent of $V$ and neglecting the image force, the function $s(y)$ will be close to unity so that $m$ is correct and nearly constant, resulting in straight line F-N plots. The change in the slope of the F-N plot upon adsorption of atoms is a measure of the change in the work function ($\Delta\varphi$). The change in the $\beta$ factor and the emitting area $A$, if any, is reflected in the pre-exponential term of the complete F-N equation.

The electric field involved in the field emission process has a magnitude of approximately $10^7$ V/cm for metals that have a work function varying from 3-5 eV. It is clearly not possible or even not desirable to obtain field emission by applying such intense voltages. These high voltages been achieved by exploiting the emitter geometry to make it sharp; as the field increases with increasing curvature, the applied voltage is kept constant. This forms an important application of this emission process, which is widely known as the field emission microscope (FEM).